ELECTRON MICROPROBE ANALYSES OF KARSTIC AND LATERITIC BAUXITES

by

J. HIDASI and P. MENSÁROS

Department of Applied and Engineering Geology, Eötvös University, Budapest

Received: 15 March 1974

SUMMARY AND CONCLUSIONS

On the basis of the studies made on the available sections, the main difference between the karstic and lateritic bauxites – owing to the deposition and accumulation localities and circumstances – is the presence of globular elements in the former, and occurence of fluidal texture and veins in the latter type. The position and form may suggest different material-movements in the same time. The difference arises from the direction of these movements.

The formation of the globular elements, which are dominant in the karstic bauxites, can be due mainly to the parallelly directed massive movement of this colloidal material. The globular elements show – even in thin-section studies – significant differences, which are represented also in the element distribution. These differences enable to separate the pisoid generations, and the genetic bases of these generations are the changed chemical circumstances of the certain intervals. These differences, namely, are sufficiently great to suggest the distant formation of the pisoids and ooids. Their can be explained by redeposition. It is proved also by the standpoints founded for the classification of the pisoids and ooids in our previous studies, and by Fig. 14 to 21., obtained during the electron microprobe analyses. The Mn-rich particle containing Ni, Co and Ti, resembles in its element composition the frequently occuring Mn crust of the bauxite footwalls. On the basis of the analysis, this grain seems to be related to this crust beneath the bauxite bodies.

The underlying rock of the bauxite is Dachsteinkalk, the overlying rock is the Upper Cretaceous spotted marl. The Mn-rich grain came from the middle portion of the bauxite body. Consequently this grain derived from the Mn-crusted footwall of a previously formed then eroded bauxite body, and proves unequivocally the allochtonous character of this bauxite.

The veins recognized in lateritic bauxites show epigenetic processes (pyritization, pyrite decomposition).

In the lateritic bauxites the fluidal textural elements, veins are characteristic. These are directed vertically, in which the solutions also moved in vertical direction. The solutions mobilized the Fe, and in the course of the downward motion this Fe precipitates by the changed chemical circumstances, and infills the veins.

In the distribution of the studied main elements the most striking differences were shown by the Fe. In the case of the karstic bauxites of Hungary the Fe distribution is rather regular – as suggested by the macroscopically visible red colour. In lateritic bauxites the Fe concentration varies within wide extremes. Locally the total abcence of Fe occurs (on the white- or yellow-coloured points of the bauxite). Similar essential differences do not appear in the Al, Si and Ti distribution. The reversed enrichments of the Al and Fe is characteristic in both cases.

In the textural studies the electron microprobe analyses were essentially useful to trace textural elements, wich are inseparable in thin-sections or spectroscopic examinations. The electron microprobe analysis naturally is insufficient for mineral determination,

because its results are element compositions. The most favourable way, in the case of the textural analysis of bauxites, is the accompained use of both thin-section and electron microprobe studies.

Preparation of samples and short description of the method

Electron microprobe analysis requires suitably prepared samples. Owing to the low hardness, loose and heterogenic texture, high porosity and hydrous minerals, the Hungarian bauxites are not convenient for thin-section or surface-section preparation.

The samples were prepared for electron microprobe analysis in the Laboratory for Geochemical Research of the Hungarian Academy of Sciences. After mounting in Araldit-H and Palatal-4 plastics the dry coarse-grinding was made on SiC abbrasive cloth (320, 600 mesh). In every cases the grinding was carried out manually. The final surfacial polishing was made on cloth, with Al_2O_3-water pulp. In this way score-free, but slightly uneven surfaces were obtained. The removing of the grinding materials, remained in the small surfacial hollows, required a some minute ultrasonic cleaning. The surface sections, prepared in this way need conducting. The conducting material is a copper layer (about 100 Å), coated in vaacum concentrator. The conductivity between this conducting layer and the sample holder was furnished by Dotit suspended silver painting.

The analyses were carried out in the Laboratory for Geochemical Researches of the Hungarian Academy of Sciences, under the direction of Dr. G y. P a n t ó. The surface of the preparation is scanned by electronic pencil in vacuum. The samples can be studied with the following electron pictures occured on the cathode-ray tubes (only the pictures used in this present studies are listed here):

1. *Back-scattered electron picture.* The picture is built by the greater energy reflected electrons. The fields of the greater mean atomic weights (stronger electron reflection capacity) are brighter on the pictures. The following two types exsist:

a) composition picture. The position of the two detector heads is to add the reflected electrons, and the topographic effect decreases in this way.

b) topographic picture. It is a picture built up by the difference of the two detector heads' signals, bringing mainly the "relief" of the surface.

2. *Scanning picture.* The electron radiation induces characteristic X-ray radiation in the material. This element-specific X-ray radiation is detected by two variable induce detectors. These can be stepped to the characteristic wave-length of the element to be studied, and can be recognized on the cathode-luminescent screen.

a) element-distribution radiograph. The frequency and intensity of the scintillating points on the screen show the position and concentration of the represented element.

b) line profiles. The scanning takes place along predetermined lines and results in curves.

Textural studies

The graphs presented in the first part were made from Hungarian karstic bauxite of Halimba. Fig. 1. shows the composition picture of a detail from an oolite. From left to right the matrix, the crust and the core are visible. The matrix is a field of low atomic weight. Within the crust the crustal limits are well visible. The core is a bright, light field, suggesting great atomic weight. Within the core and the crust there are well isolated detrital grains, which were more sharply and distinctly shaped on the screen.

Figs. 2., 3. and 4. show respectively Al, Fe and $Ti_{K\alpha}$X-ray scanning pictures of this composition picture. The three different fields (matrix, crust, core) can be separated also on the basis of these pictures. The enrichment of Al is opposited by that of Fe. It can be proved, that this is an ooid with a core rich in iron and poor in aluminium. The matrix is Al-rich Fe-poor. The crustal part do not show in the element concentration of the X-ray scanning picture the distinct "striate" structure, visible on the composition picture. Si shows a constant, Ti a punctual distribution, and do not follow the Fe enrichment. Two groups are separable:

1. Grains smaller than 10 μm. These are most probably of autigene origin (Bárdossy and Pantó 1971).
2. Aggregations greater than 10 μm. These are well identifiable to the pronounced, bright granules mentioned at the composition picture. These are poor in Al, Fe and Si, but their Ti-content is high. As of other elements, significant enrichment cannot be recognized. Most probably these are some TiO_2 modifications (anatase or rutile). As it is visible on the composition picture, these are not crystallized forms, showing the non-autigene, but rather the detrital origin in this way. (The basis is the work of Bárdossy and Pantó 1971.) The lack of required roundness can be due to the small (about 10 to 20 μm) size of the particles.

Figs. 5. and 6. show the line distribution of the Mn and Ni. The Mn enriches in the crust and in the core, but do not follow certainly the rhythmic alteration of the crustal parts. The Ni-content increases in the direction of the core, attaining here decreases, then decreases again. Figs. 7. and 8. (composition picture and $Al_{K\alpha}$X-ray scanning picture, respectively) show an interesting phenomenon. In the textural studies it was severally recognized the deformation of the ooids, which resulted from external, mainly mechanical effects; thus fragmented, cracked or scoured specimens occured. A rare example of these deformed ooids can be seen here. Since the number of the crustal limits is constant, the crustal layers probably were condensed and depressed by the own weight of the oolite, in its plastic state.

PLATE I.

Fig. 1. Ooid. Halimba III. bauxite body.
Composition picture. Picture-width: 0,1 mm

Fig. 2. $Al_{K\alpha}$ X-ray scanning picture

Fig. 3. $Fe_{K\alpha}$ X-ray scanning picture

Fig. 4. $Ti_{K\alpha}$ X-ray scanning picture

Fig. 5. $Mn_{K\alpha}$ line profile

Fig. 6. $Ni_{K\alpha}$ line profile

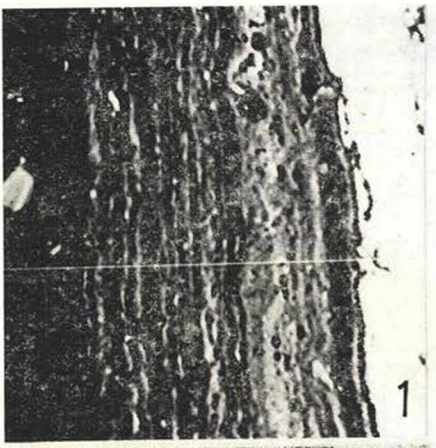
1

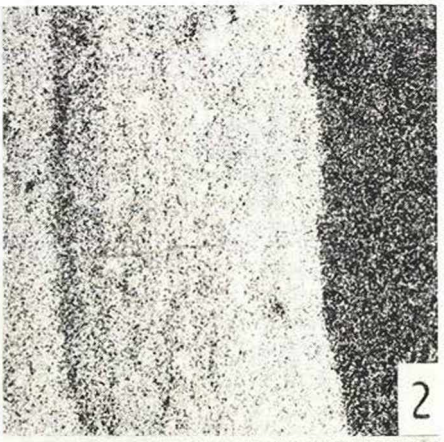
2

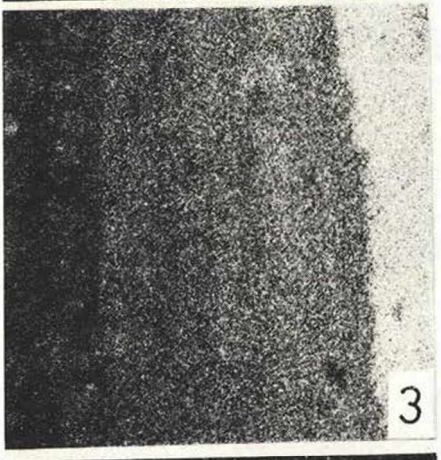
3

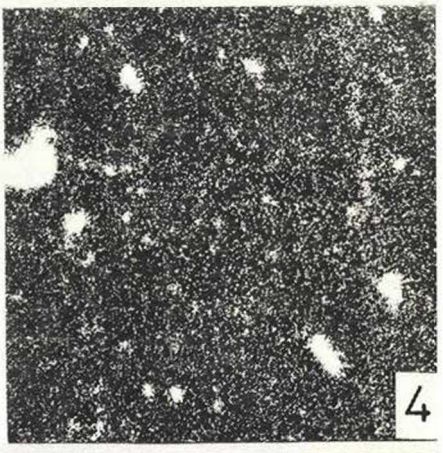
4

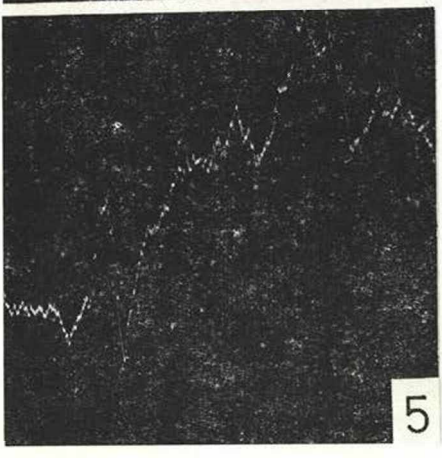
5

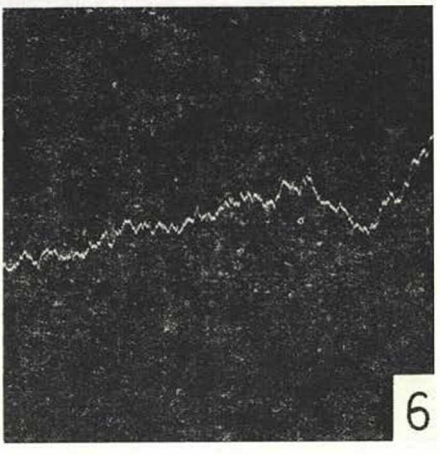
6

PLATE II.

Fig. 7. Deformed ooid. Halimba III. bauxite body.
Composition picture. Picture-width: 0,2 mm

Fig. 8. $Al_{K\alpha}$X-ray scanning picture

Fig. 9. Ooid bauxite detritus, Halimba III. bauxite body.
Composition picture. Picturewidth: 0,1 mm

Fig. 10. $Al_{K\alpha}$X-ray scanning picture

Fig. 11. $Fe_{K\alpha}$X-ray scanning picture

Fig. 12. Detrital grains, Halimba III. bauxite body.
Topographic picture. Picture-width: 0,2 mm

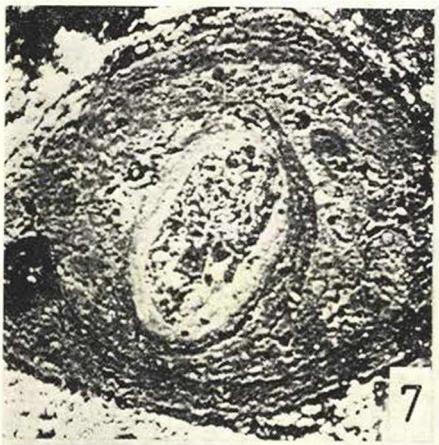
7

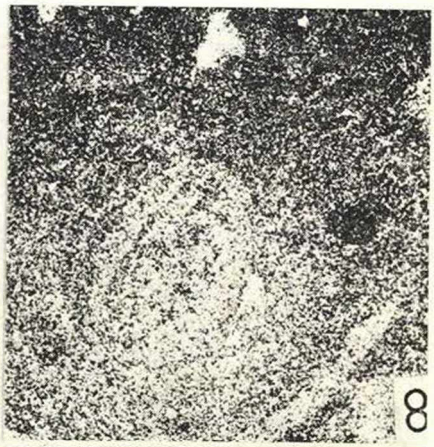
8

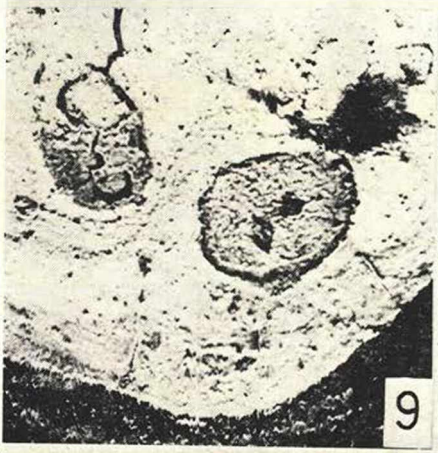
9

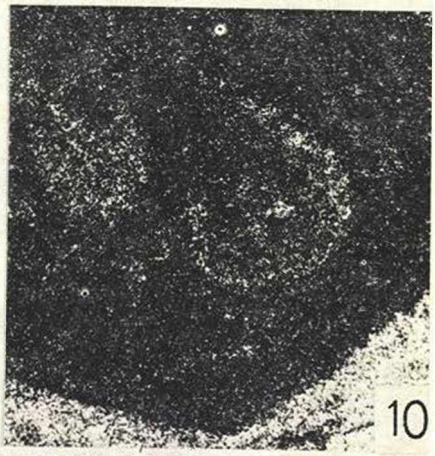
10

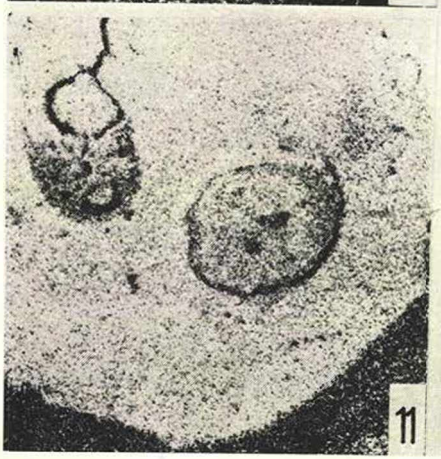
11

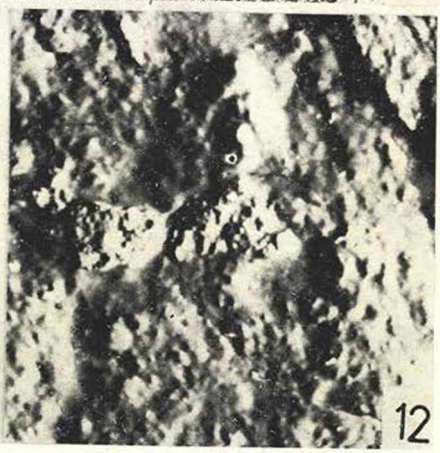
12

Fig. 9. (composition picture) and Figs 10. and 11. (Al and $Fe_{K\alpha}$ X-ray scanning pictures) show a differently deformed detrital bauxite particle. This was scoured during some movement. One of the two ooids (the lower on the figures) is of double-cored. The texture is simple; it is ranged into the ooid-group with continuous transition from the core to the crustal limit.

The next series was made from two crystal grains. On Fig. 12. (topographic picture) the well emerged, i.e. harder, rounded grains are well visible. The back-scattered electron picture (Fig. 13.) shows, that the two grains bear different element composition, and it was proved also by the X-ray scanning picture (the composition picture shown on Fig. 14. is the enlarged variety of Fig. 12.). On Fig. 15. ($Al_{K\alpha}$X-ray scanning picture) the matrix shows a nearly uniform distribution. In the grain of grater mean atomic weight the Al concentration is lower than in the other, close to that. On the $Fe_{K\alpha}$X-ray scanning picture (Fig. 16.) the Fe shows a less uniform enrichment as compared to the Al. The two mineral grains essentially different, because the former, Al-poor grain is rich in Fe, while the latter contains less Fe than the matrix. On the $Mn_{K\alpha}$X-ray scanning picture (Fig. 17.) it is visible, that the enrichment confines to the Fe-poor grain. As compared to the matrix, the Fe-rich grain also contains Mn, but the difference of the two grains is essential. On the basis of Fig. 18 and 19. scanning pictures, the Co- and Ni-content is also high.

Ti-graphs were also made (Fig. 20.) Similarly as on Fig. 4., the Ti occurs also in the aggregates smaller than 10 μm. In comparison with the mean distribution, the Fe-rich grain shows a somewhat higher concentration. The above mentioned facts suggest, that in the two close grains enrich the geochemically related elements, but the concentrations show considerable differences. Because it is unlikely that the circumstances of the formation or the subsequent dissolution were different, these grains possibly formed in distant places, and secondary transportation came them close to each other.

On Fig. 21. the $Si_{K\alpha}$X-ray scanning picture of this same setting is shown. The Si enriches in larger aggregations, suggesting the presence of clay minerals.

The following graph-set is made on grey pyritic bauxite sample. Owing to their large size, the pisoids of this bauxite are unconvenient for the electron microprobe analysis. Besides of the size-problems, the hardness-differences of the textural elements also encumbered the preparation of suitable sections. Hence only pisoidic portion was examinable. It is visible on the composition picture (Fig. 22.), that the pisoid is not a sphaeroidal structure. It has a much greater atomic weight as compared to the matrix. In the matrix scattered small grains can be detected, with great electron reflection. On the boundary of the matrix and the globular grain there is a crust, which has a reflection identical to that of the matrix. On the $Fe_{K\alpha}$X-ray scanning picture (Fig. 23.) appears markedly the nodular Fe-enrichment of the matrix, outside of

the irregular outer crust. These small aggregations would be pyrite-marcasite grains. The Al attains its maximum in the pisoids (Fig. 24.). After a minimum in the outer crust, the Al-content increases again in the matrix. The Ca (Fig. 25.) enriches exclusively in the outer crust and in the matrix. The Ca of the matrix is represented as calcite or dolomite.

The composition picture of Fig. 26. shows a sample from the uppermost degraded zone of the Malomvölgy XII. bauxite body. The three well separable reflection fields can be traced on the X-ray scanning pictures too (Figs 27., 28., 29.). The matrix equally contains Al, Si and Fe. The dark field shows great Al content and complete Fe and Si abscence alike. This macroscopically white aggregate is gibbsite. On the basis of the element composition the matrix is of kaolinitic, and the Fe-rich part is macroscopically violet-coloured. On the other hand the Fe-free aggragate is white. This colour change, which is parallel to the Fe-content, can be due to the differences of the hematite-content. On the basis of trace element analyses, the Mn-content and the related changes in violet colour is opposed.

The sample is derived from a portion penetrated by macroscopically yellowish, 2 to 5 m long vertical veins, beneath the upper Fe crust of the Malomvölgy XII. bauxite body (Fig. 30., composition picure). On the K_{α}X-ray scanning picture (Fig. 31.) visible is that the Fe is not represented, consequently these are desironized veins.

The next graph-set was made on this same section. On the composition picture of the globular grain (Fig. 32.) it is a great atomic weight field, as can be identified with the $Fe_{K\alpha}$X-ray scanning picture (Fig. 33.). Also parallel is the Ti distribution (Fig. 34.), which occurs, similarly as in the earlier samples, in the aggregates of about 10 μm size. The Al, as compared to the Fe, enriches in the matrix (Fig. 35.).

In the following part there are presented some samples from the lateritic bauxite of Goa (India), which were available by Gy. Komlóssy (ALUTERV). Here also the distribution of the main bauxitic elements (Al, Fe, Si, Ca, Ti) were studied.

The lateritic bauxite bodies are densely penetrated by fissures. These fissures – according to the climate of the given area – are infiltrated by solutions in great quantity. From these Fe-containing solutions goethite and hematite precipitate, infilling slowly the fissures. Some graphs of this "drainage-system"-like texture are figured here (Figs 36. to 45.). This series shows the veins in cross-section. On the composition pictures the high reflection fields represent the Fe-rich infilling of the vein, and within them – where the infilling was incomplete – there are Al-rich fields with low reflection. The X-ray scanning pictures show the Fe (Figs. 38., 40., 45), the Al (Figs. 37., 41., 44.) and the Si (Fig. 42.) distribution.

On the composition picture presented on Fig. 46. a longitudinal section of a vein is shown, with the K_{α}X-ray scanning pictures of Fe (Fig. 47.), Al. (Fig. 48.) and Si (Sig. 49.). The Fe and Al enrichments here are in contrast too. On the basis of mineralogic studies the vein-

PLATE III.

Fig. 13. Detrital grains, Halimba III. bauxite body.
Composition picture. Picture width: 0,2 mm

Fig. 14. Detrital grains, Halimba III. bauxite body.
Composition picture. Picture-width: 0,1 mm

Fig. 15. Al_{K_α}X-ray scanning picture

Fig. 16. Fe_{K_α}X-ray scanning picture

Fig. 17. Mn_{K_α}X-ray scanning picture

Fig. 18. Co_{K_α}X-ray scanning picture

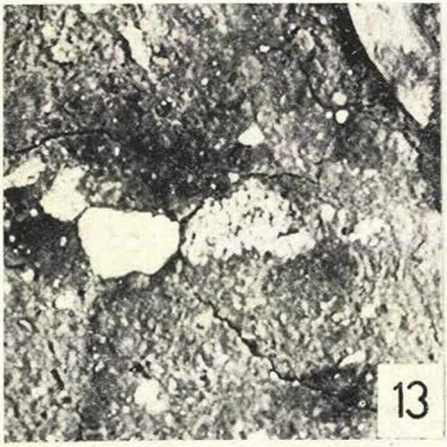
13

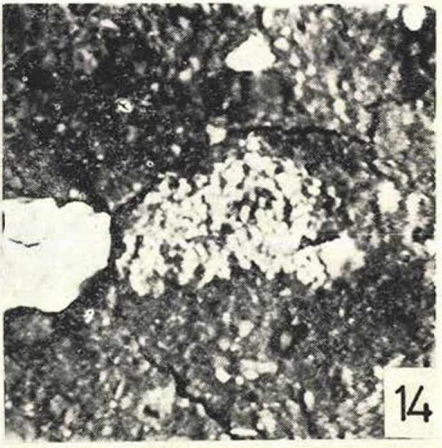
14

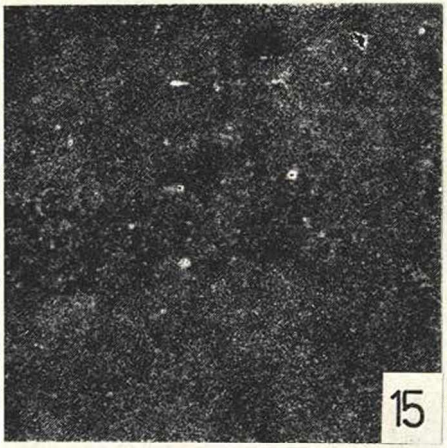
15

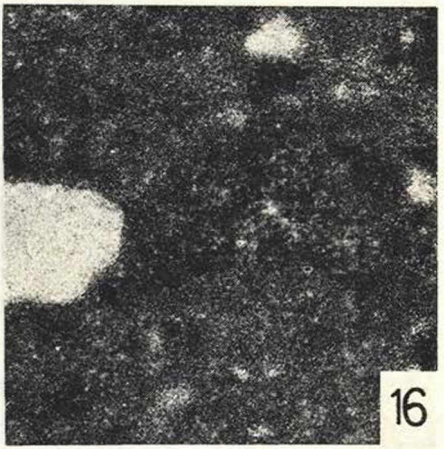
16


17

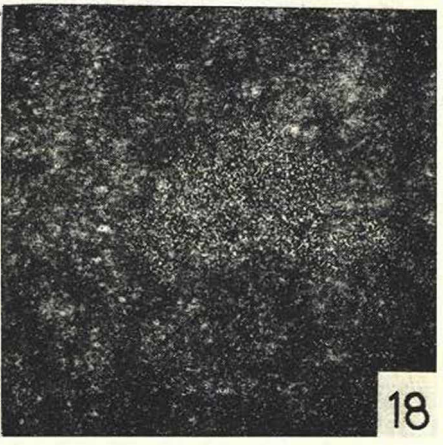
18

PLATE IV.

Fig. 19. Ni_{K_α}X-ray scanning picture

Fig. 20. Ti_{K_α}X-ray scanning picture

Fig. 21. Si_{K_α}X-ray scanning picture

Fig. 22. Pisoid from pyritic bauxite, Halimba III. bauxite body. Composition picture. Picture width: 0,2 mm

Fig. 23. Fe_{K_α}X-ray scanning picture

Fig. 24. Al_{K_α}X-ray scanning picture

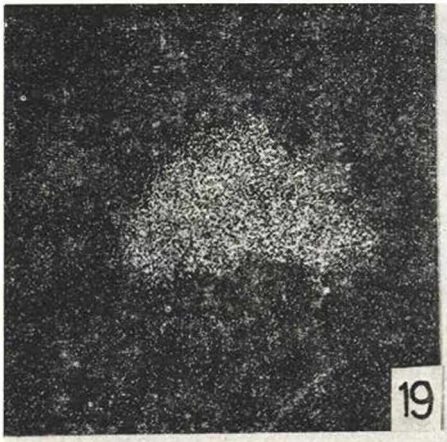
19

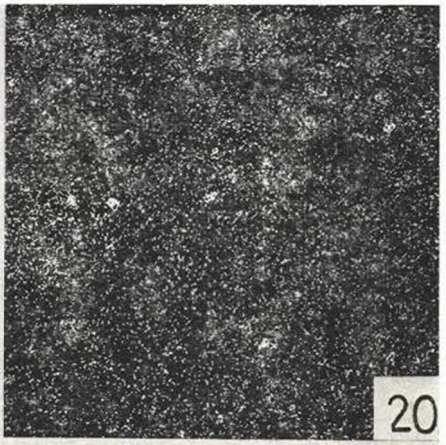
20

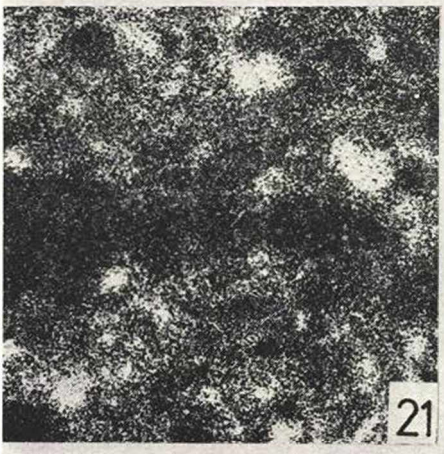
21

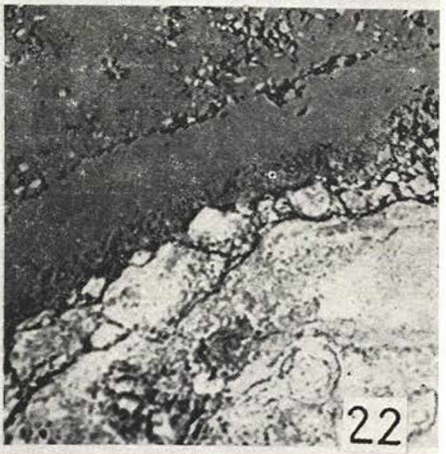
22


23


24

PLATE V.

Fig. 25. Ca_{K_α}X-ray scanning picture

Fig. 26. Degraded bauxite, Halimba Malomvölgy XII. bauxite body.
Composition picture. Picture-width: 0,2 mm

Fig. 27. Al_{K_α}X-ray scanning picture

Fig. 28. Si_{K_α}X-ray scanning picture

Fig. 29. Fe_{K_α}X-ray scanning picture

Fig. 30. Desironized vein in bauxite,
Halimba Malomvölgy XII. bauxite body.
Composition picture. Picture-width: 0,2 mm

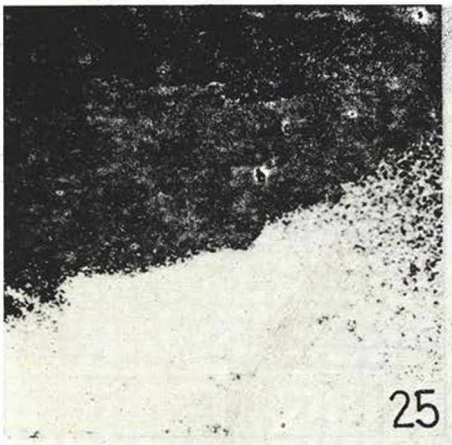
25

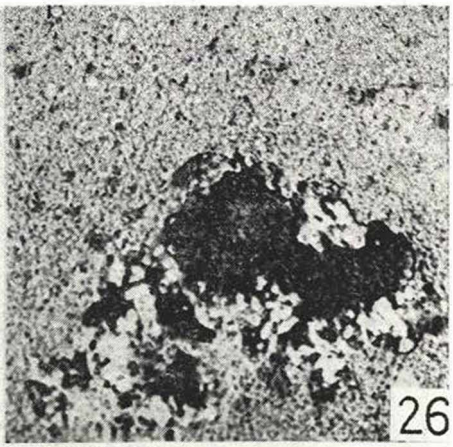
26

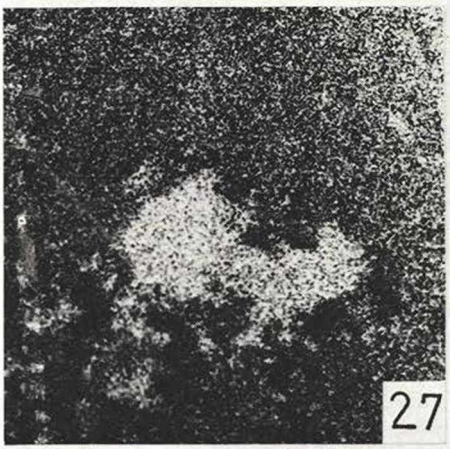
27

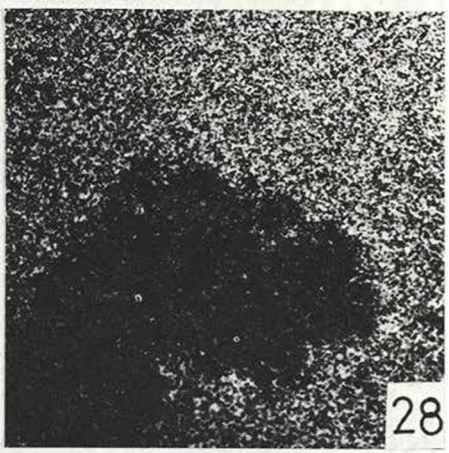
28

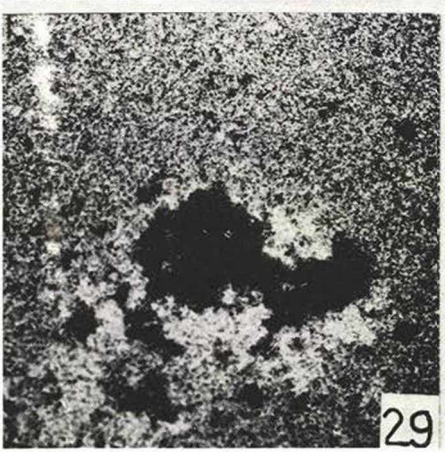
29

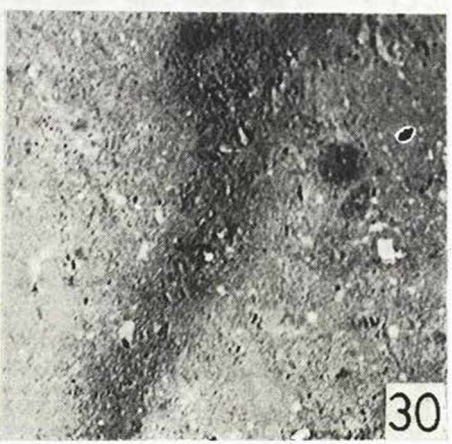
30

PLATE VI.

Fig. 31. $Fe_{K\alpha}$X-ray scanning picture

Fig. 32. Globular grain in bauxite, Halimba Malomvölgy XII. bauxite body.
Composition picture. Picture-width: 0,2 mm

Fig. 33. $Fe_{K\alpha}$X-ray scanning picture

Fig. 34. $Ti_{K\alpha}$X-ray scanning picture

Fig. 35. $Al_{K\alpha}$X-ray scanning picture

Fig. 36. Fe-rich vein-infilling, Goa, Shakti.
Composition picture. Picture-width: 0,2 mm

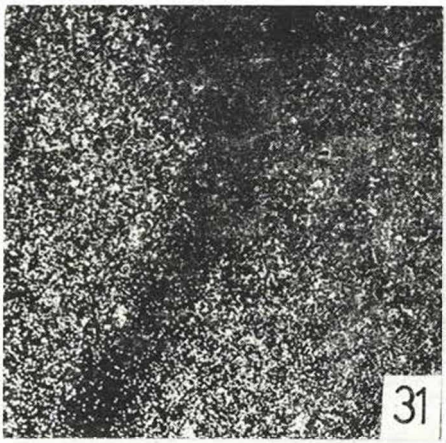
31

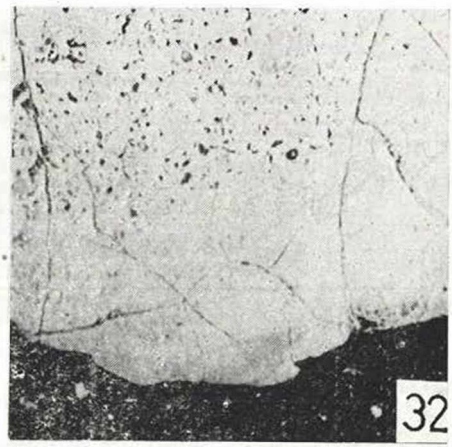
32

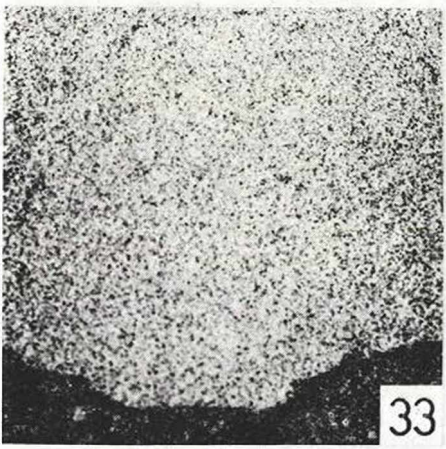
33

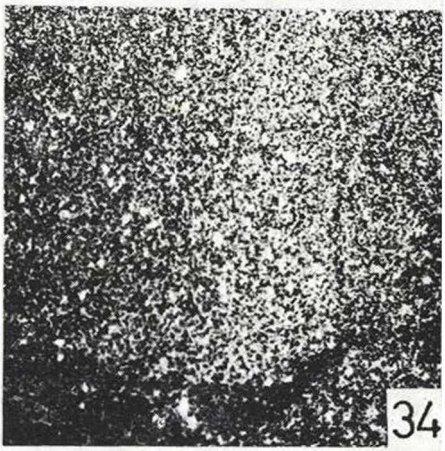
34

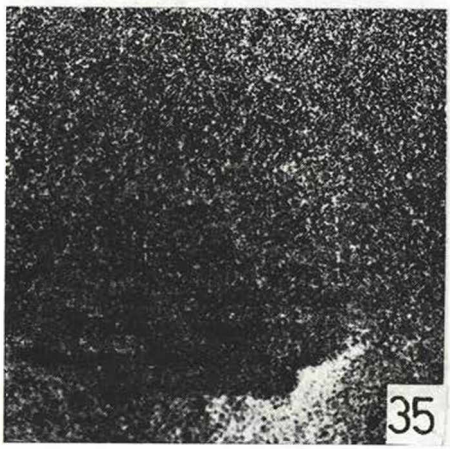
35

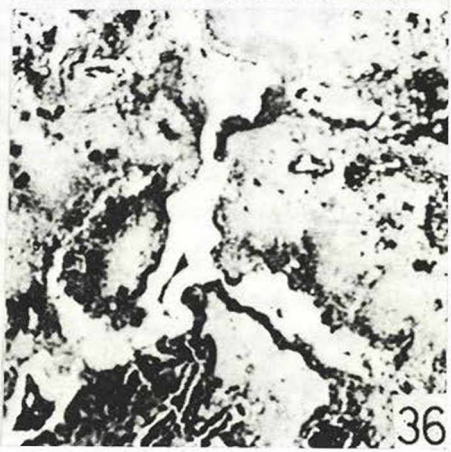
36

PLATE VII.

Fig. 37. $Al_{K\alpha}$X-ray scanning picture

Fig. 38. $Fe_{K\alpha}$X-ray scanning picture

Fig. 39. Fe-rich vein-infilling, Goa, Shakti. Composition picture. Picture-width: 0,2 mm

Fig. 40. $Fe_{K\alpha}$X-ray scanning picture

Fig. 41. $Al_{K\alpha}$X-ray scanning picture

Fig. 42. $Si_{K\alpha}$X-ray scanning picture

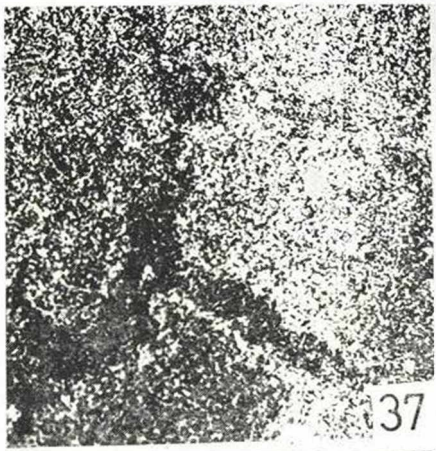
37

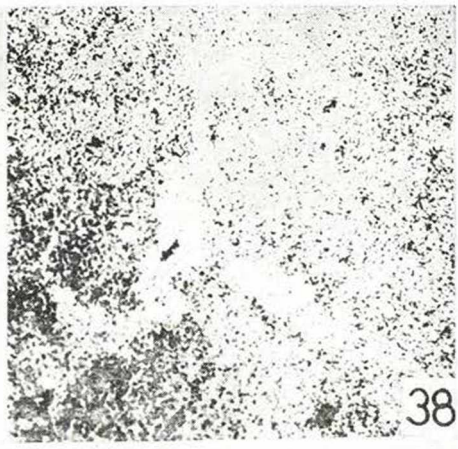
38

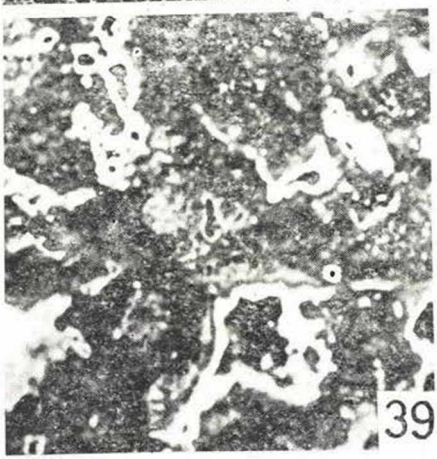
39

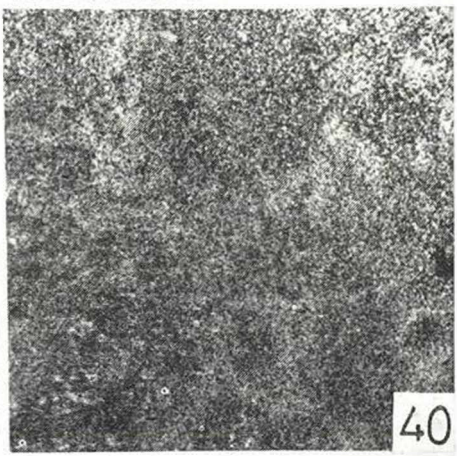
40


41

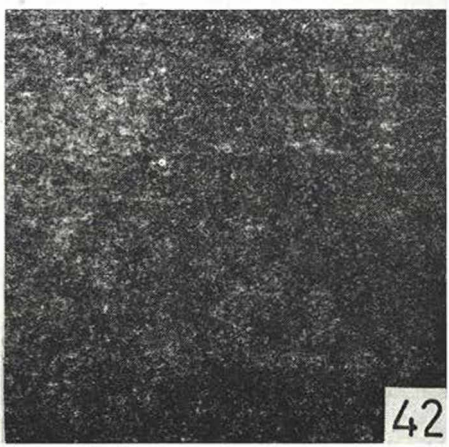
42

PLATE VIII.

Fig. 43. Fluidal vein-infilling, Goa, Shakti.
Composition picture. Picture-width: 0,2 mm

Fig. 44. Al_{K_z}X-ray scanning picture

Fig. 45. Fe_{K_z}X-ray scanning picture

Fig. 46. Longitudinal vein section, Goa, Junas.
Composition picture. Picture-width: 0,2 mm

Fig. 47. Fe_{K_z}X-ray scanning picture

Fig. 48. Al_{K_z}X-ray scanning picture

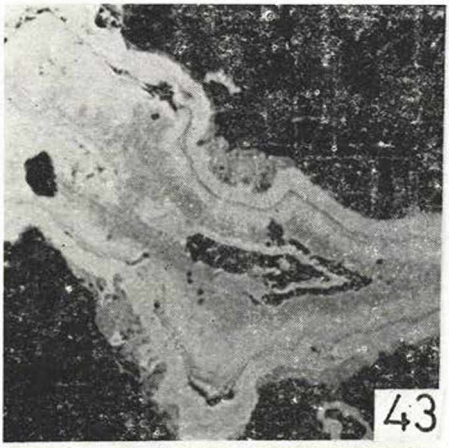
43

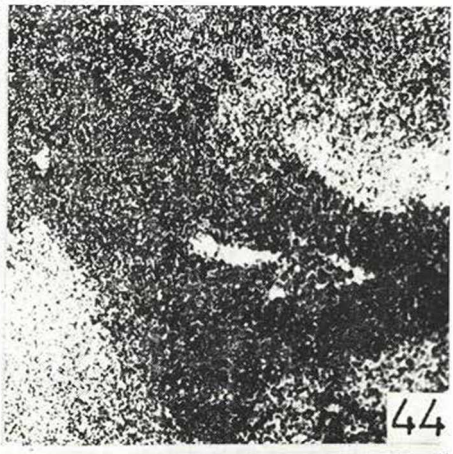
44

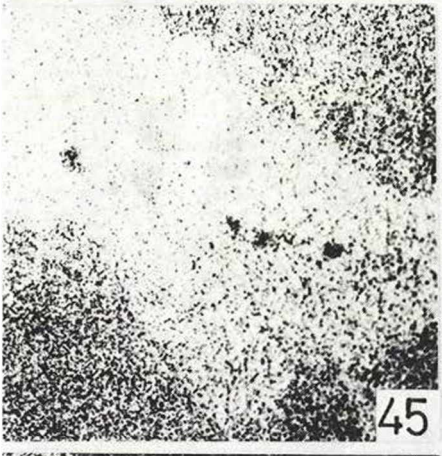
45

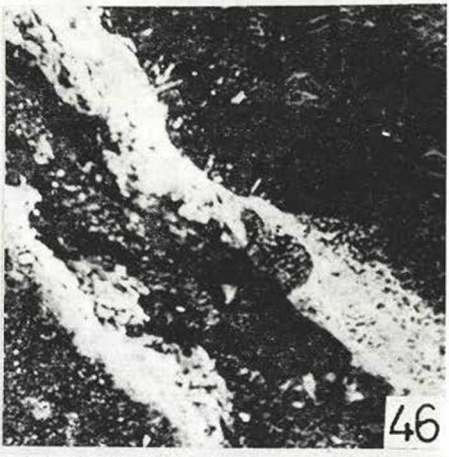
46

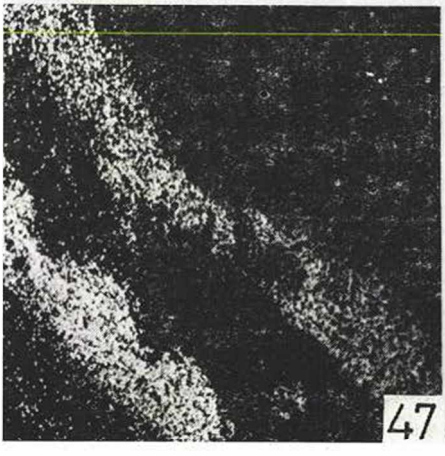
47

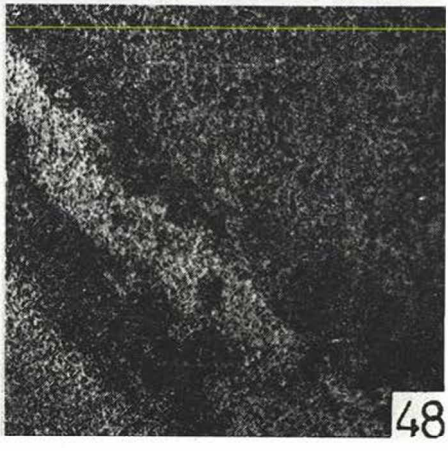
48

PLATE IX.

Fig. 49. $Si_{K\alpha}$X-ray scanning picture

Fig. 50. Detrital grain, Goa, Junas.
Composition picture. Picture-width: 0,15 mm

Fig. 51. $Ti_{K\alpha}$X-ray scanning picture

Fig. 52. $Fe_{K\alpha}$X-ray scanning picture

Fig. 53. $Al_{K\alpha}$X-ray scanning picture

Fig. 54. Detrital grains, Goa, Junas.
Composition picture. Picture-width: 0,075 mm

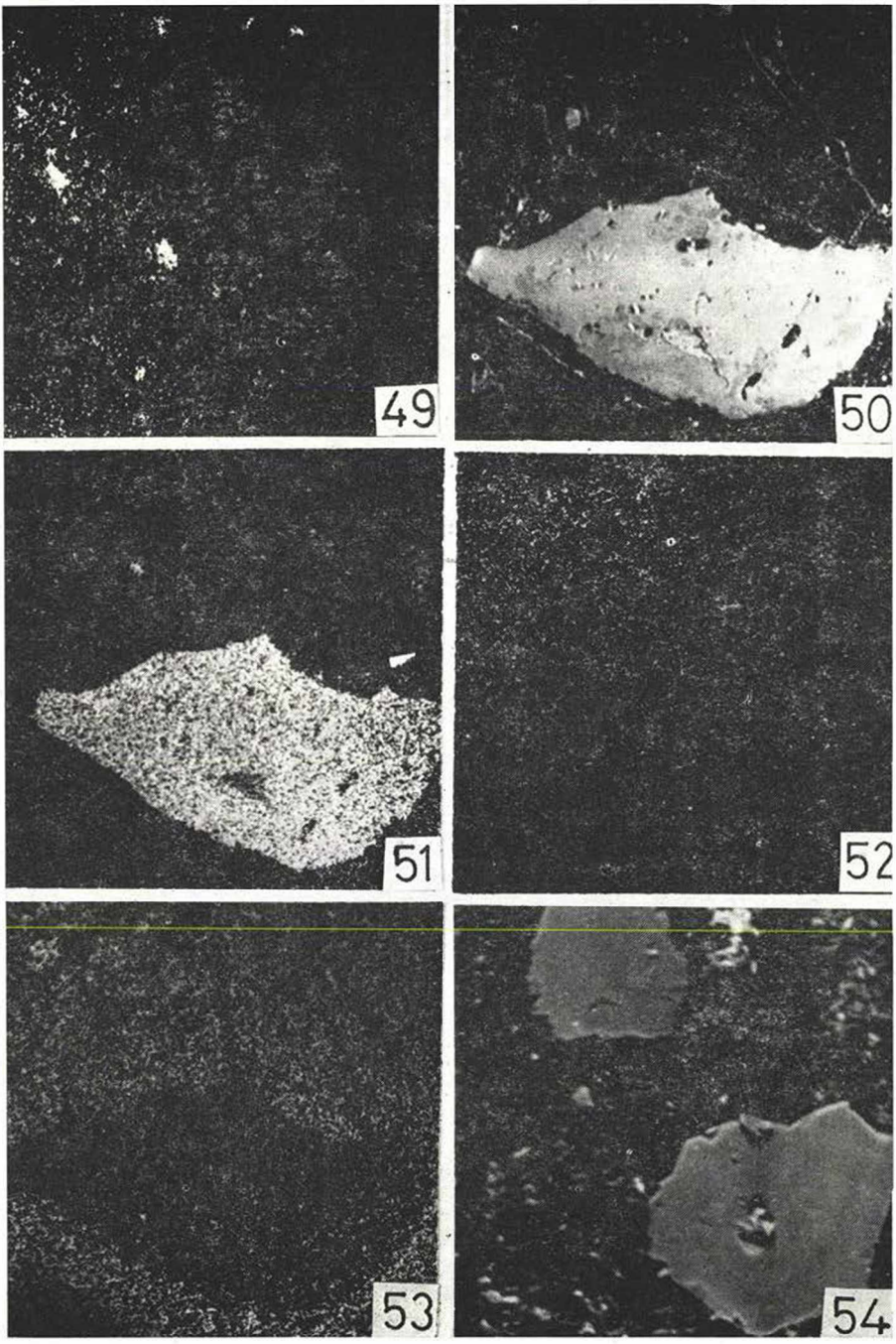
49
50
51
52
53
54

PLATE X.

Fig. 55. Mg_{K_α}X-ray scanning picture

Fig. 56. Si_{K_α}X-ray scanning picture

Fig. 57. Al_{K_α}X-ray scanning picture

Fig. 58. Fe_{K_α}X-ray scanning picture

Fig. 59. Detrital grains, Goa, Shakti.
Composition picture. Picture-width: 0,2 mm

Fig. 60. Ti_{K_α}X-ray scanning picture

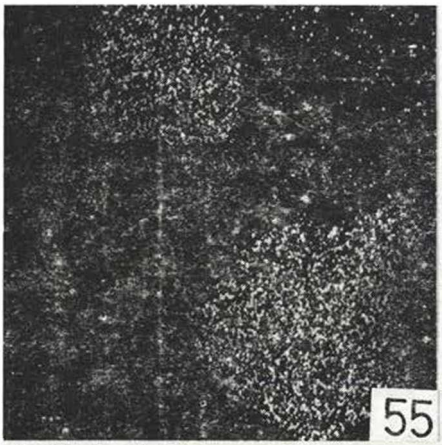
55

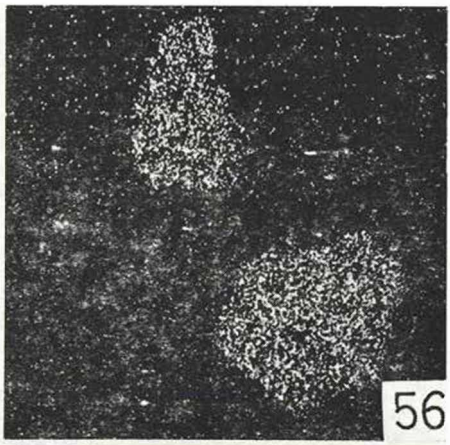
56

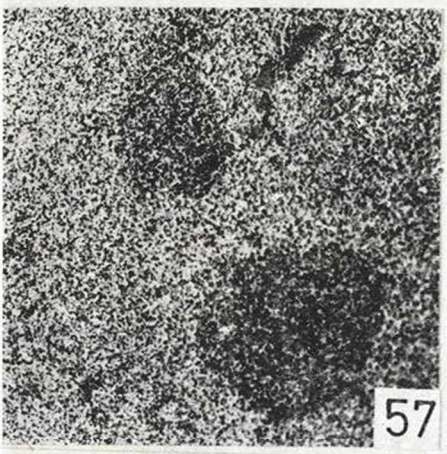
57

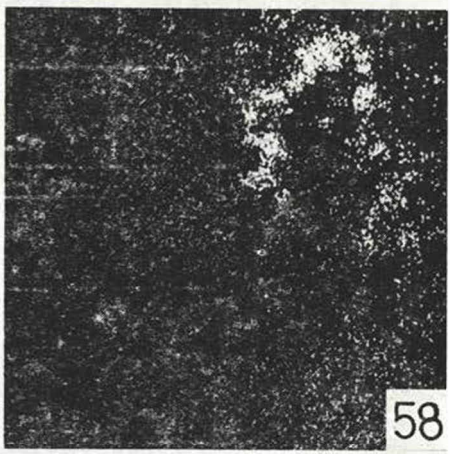
58


59

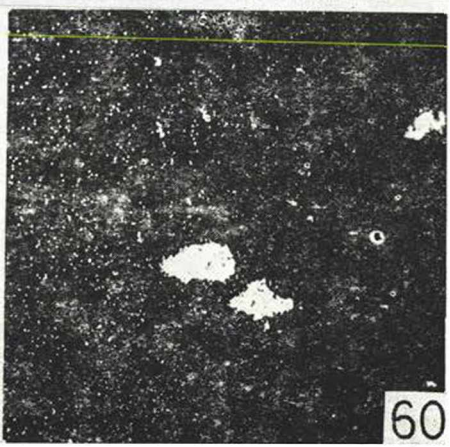
60

infilling within the Fe crust is gibbsite. The Si enriches in the matrix. The Si is connected rather to Al-rich parts then to the Fe-rich fields.

On the basis of corresponding Ti (Fig. 51.), Fe (Fig. 52) and Al (Fig. 53.) K_{α}X-ray scanning pictures of composition picture figured on Fig. 50., a high Ti-content mineral grain can be recognized. It is neither an ilmenite, so characteristic in bauxites by the poor Fe-content, nor ulvite (Fe_2TiO_4) and pseudobrookite. The lack of Si excludes the presence of any silicate. Hence this mineral grain may be a TiO_2 modification (anatase or rutile).

Finally two mineral grains are presented on the Fig. 54. composition picture. These bear a lower reflection as compared to the TiO_2 modification mentioned above. On the basis of Fig. 55. $Mg_{K_{\alpha}}$X-ray scanning picture, Mg-content appears, but enrichment exclusively occurs in Si (Fig. 56.). The Fe-content is greater than that of the matrix. Na, K and Ca-content cannot be detected. Considering the element composition and the form, these grains can be determined as Ca-less amphiboles.

REFERENCES

Balkay, B. and Bárdossy, Gy. (1967): Lateritesedési részfolyamat vizsgálata Guinea-i lateriteken. (Étude des processus élémentaires de la latérisation sur latérites guinéennes.) Földt. Közl. XCVII. 1. pp. 91–101.

Bárdossy, Gy. (1961): A magyar bauxit geokémiai vizsgálata. (Geochemical research of Hungarian bauxites). MÁFI kiadványa.

Bárdossy, Gy. and Pantó, Gy. (1970): A bauxitok vizsgálata elektronmikroszondával. (Research of bauxites by electron microprobe.) BKL Bányászat, 103, 2. pp. 825–837.

Bárdossy, Gy. and Pantó, Gy. (1972): On the pyrite types in bauxites. Acta Geol. tom. 16. pp. 3–11.

Dudich, E. Jun. and Komlóssy, Gy. (1969): Ősföldrajzi-szerkezeti szempontok a magyar bauxit korkérdéséhez. (Considérations paléogeographiques et tectoniques sur la probleme de l'age des bauxites en Hongrie.) Földt. Közl. XCIC. 2. pp. 155–165.

Komlóssy, Gy. (1966): A bauxit piritesedés kérdése. (On the problem of the pyritisation of bauxite.) Földt. Közl. XCVI. 2. pp. 220–226.

Pantó, Gy. (1969): Elektronmikroszonda működése és földtani vonatkozásai. (Working of the electron microprobe and its geological application.) MTA X. Oszt. Közl. 3. pp. 263–281.